Physical and spurious modes in mixed finite element formulation for the Galbrun equation

Felix Dietzsch[1], Luis Hervella-Nieto[2], Steffen Marburg[3*], Rodolfo Rodríguez[4], Hannah Weisbecker[5]

[1] *Institut für Energieverfahrenstechnik, Chemieingenieurwesen, TU Bergakademie, Freiberg, Germany*
[2] *Facultade de Informática, Universidade de A Coruña, A Coruña, Spain*
[3] *LRT4 – Institute of Mechanics, Universität der Bundeswehr München, D-85579 Neubiberg, Germany*
[4] *CI²MA, Departamento de Ingeniería Matemática, Universidad de Concepción, Concepción, Chile*
[5] *Institut für Festkörpermechanik, Technische Universität Dresden, 01062 Dresden, Germany*

SUMMARY

Sound propagation in moving media can be described by Galbrun equation for the oscillating component of the fluid displacement. A displacement based finite element formulation using standard Lagrangian elements produces spurious modes. Investigations in literature (e.g., IJNME 63, 974-987, 2005) have shown that Mini elements and Taylor-Hood elements suppress the effect of spurious modes. Herein, the quadratic eigenvalue problem for the mixed formulation in 2D using Mini and Taylor-Hood elements is solved. Solution confirms former results such that both element types are suitable for low Mach numbers and under certain conditions. Although the formulation is not free from spurious results, physical and spurious modes are well separated for low Mach numbers in non-dissipative systems. As reported, mini elements produce spurious modes for Mach numbers > 0.5 whereas Taylor-Hood elements perform more stable even for large Mach numbers in non-dissipative systems. If absorbing walls are considered, separation of physical and spurious modes becomes less clear. Then, eigenvalues of both types of modes are located closer to each other in the complex plane. Examples encompass the 1d duct problem, for which the spurious modes are discussed for the energy conserving problem, and an annular duct for which the dissipative case is investigated.

KEY WORDS: Galbrun equation; mixed finite element fomulation; spurious modes; sound propagation in flow

1. INTRODUCTION

For many aeroacoustic problems such as jet noise, duct acoustics and liner design, a main focus lies on the prediction of sound propagation in nonuniform flow, see for example [1, 3]. Mathematically, such problems are often described by the linear Euler equations (LEE). However, acoustic problems with ambient flow can also be modeled by using Galbrun equation, which was first derived by Galbrun in 1931 [9]. This is a second order linear partial differential equation describing the sound propagation in terms of a displacement perturbation as the only variable. For practical use, a mixed formulation in terms of displacement and pressure perturbation is used. Despite of using these two variables for solution, there is still a gain of variables compared to the conventional system of equations. A further advantage of the Galbrun equation is the existence of an exact expression for acoustic energy and intensity [10]. Furthermore, boundary conditions and coupling conditions are easily formulated [8].

The solution of the eigenvalue problem of the Galbrun equation can help to better understand the phenomenon of sound propagation in the presence of ambient flow. Especially in the case of

*Correspondence to: Steffen Marburg, LRT4 – Institute of Mechanics, Universität der Bundeswehr München, D-85579 Neubiberg, Germany, Email: steffen.marburg@unibw.de

swirling mean flows, Galbrun formulation seems to be an interesting alternative since an often used simplification of the LEE, the so called full-potential formulation, is not applicable. A few papers [6–8, 16–18, 22, 23] deal with solving Galbrun equation using the finite element method (FEM). However, none of these works explicitly addresses the solution of the eigenvalue problem. Among other applications, solution of the eigenvalue problem is relevant for intonation of musical woodwind instruments. While traditionally analyzed only experimentally, application of numerical methods has been approaching this class of instruments in recent years. Two examples of these applications to woodwind instruments are known by Fuß et al. [5] for the recorder and by Richter et al. [21] for the bassoon.

In this study, the quadratic eigenvalue problem resulting from the discretization of Galbrun equation is solved by means of a FEM. A mixed element formulation is chosen that satisfies the inf-sup condition in the no-flow case. Satisfaction of the inf-sup condition by these formulations for non-vanishing flow has remained open. Treysséde et al. [23] showed that spurious modes are not observed when Mini elements or Taylor-Hood elements are used. The paper by Gabard et al. [7] indicates that spurious modes can be observed for Mini elements at large Mach numbers, in particular for Mach numbers greater than 0.5. Taylor-Hood elements performed more stable even at large Mach numbers. It remained unclear whether these formulations are actually free of spurious modes or not. The authors of this article could not find any indication in the literature where the eigenvalue problem of Galbrun equation has been investigated for a finite element model.

It is demonstrated in this study why Taylor-Hood elements perform well for weakly damped problems. Previous results for Mini elements are confirmed and, for higher Mach numbers, real eigenvalues of spurious character are evaluated. Nevertheless, spurious modes are found in all cases except for the no-flow case. For Taylor-Hood elements, these eigenvalues occur in regions far (enough) away from the real axis. Furthermore, it is shown that problems with large regions of absorption (e.g., exterior acoustic problems) do not easily allow the separation between physical and spurious modes. In these cases, special techniques are required to identify the relevant physical modes.

The outline of the paper is as follows. Galbrun equation is recalled in Section 2. Then, a mixed formulation of the corresponding eigenvalue problem is given. We end this section with a brief description of the finite elements used to solve this problem. In Section 3, we consider as a first test the sound propagation inside a one-dimensional duct with rigid walls. A constant ambient pressure and a steady ambient flow velocity are assumed. In this case, the analytical solution is known and this allows us to assess the effectiveness of the used finite element methods. A similar problem but now posed inside an annulus with partially absorbing boundary conditions is solved as a second test in Section 4. In spite of the bounded character of the domain, the configuration of this test is similar to that of an exterior problem. Finally, we draw some conclusions in Section 5.

2. THEORETICAL ASPECTS

2.1. Galbrun equation

The equation for an acoustic problem with ambient flow in terms of the oscillatory displacement $\boldsymbol{w}$, also referred to as the Galbrun equation, can be written as

$$\rho_0 \frac{d^2\boldsymbol{w}}{dt^2} + (\boldsymbol{\nabla}\cdot\boldsymbol{w} + \boldsymbol{w}\cdot\boldsymbol{\nabla})\boldsymbol{\nabla}p_0 - \boldsymbol{\nabla}(\rho_0 {c_0}^2 \boldsymbol{\nabla}\cdot\boldsymbol{w} + \boldsymbol{w}\cdot\boldsymbol{\nabla}p_0) = \boldsymbol{0}. \tag{1}$$

Herein, p_0, ρ_0, and c_0 represent the ambient pressure, mass density and speed of sound, respectively. A detailed discussion on the derivation of Galbrun equation can be found in [10] and [20].

For numerical analysis, the values of the ambient variables p_0, ρ_0, and c_0, are assumed to be constant. This simplifies Galbrun equation to

$$\rho_0 \frac{d^2\boldsymbol{w}}{dt^2} - \rho_0 {c_0}^2 \boldsymbol{\nabla}(\boldsymbol{\nabla}\cdot\boldsymbol{w}) = \boldsymbol{0}. \tag{2}$$

Note that $d\boldsymbol{w}/dt$ accounts for the material time derivative which is determined as

$$\frac{d(\cdot)}{dt} = \frac{\partial(\cdot)}{\partial t} + \boldsymbol{v}_0 \cdot \boldsymbol{\nabla}(\cdot), \tag{3}$$

where we assume a steady ambient flow velocity $\boldsymbol{v}_0$. For constant speed of sound c_0 and constant ambient density ρ_0, Equation (2) looks similar to the Pierce equation for the velocity potential [19]. However, the Pierce equation is a generalized scalar wave equation whereas our simplified Galbrun equation remains a vector equation. The Mach number as normalized velocity is related to the ambient flow velocity and the speed of sound as

$$Ma = \frac{|\boldsymbol{v}_0|}{c_0}\,. \tag{4}$$

Furthermore, a harmonic time dependence $e^{-i\omega t}$ is assumed for oscillatory quantities, in particular for the displacement $\boldsymbol{w}$ and for the (sound) pressure p. Application of harmonic time dependence to Equation (2) yields

$$-\rho_0\omega^2\boldsymbol{w} - 2i\omega\rho_0\boldsymbol{v}_0 \cdot \boldsymbol{\nabla}\boldsymbol{w} + \rho_0\boldsymbol{v}_0 \cdot \boldsymbol{\nabla}(\boldsymbol{v}_0 \cdot \boldsymbol{\nabla}\boldsymbol{w}) - \rho_0{c_0}^2\boldsymbol{\nabla}(\boldsymbol{\nabla} \cdot \boldsymbol{w}) = \boldsymbol{0}. \tag{5}$$

If not mentioned otherwise, a rigid surface boundary condition will be regarded in the numerical simulation. At a motionless and rigid surface the normal component of the oscillatory displacement has to vanish, i.e.,

$$\boldsymbol{w} \cdot \boldsymbol{n} = 0, \tag{6}$$

where $\boldsymbol{n}$ is the unit outward normal. The implementation of this boundary condition for the Galbrun equation is much simpler than for the Helmholtz equation, because the displacement is an explicit variable, contrary to the pressure.

In the second numerical example of this study, an admittance boundary condition is applied to consider the effect of absorption. Assuming constant ambient pressure, a boundary admittance Y, and vanishing flow in the direction normal to the boundary (i.e., $\boldsymbol{v}_0 \cdot \boldsymbol{n} = 0$), the admittance boundary condition can be formulated as

$$-i\omega\boldsymbol{w} \cdot \boldsymbol{n} = Yp = \frac{\tilde{Y}p}{\rho_0 c_0}, \tag{7}$$

where $\tilde{Y}$ represents a normalized boundary admittance. For a detailed discussion of different boundary conditions we refer to [10].

2.2. Weak formulation and polynomial eigenvalue problem

It has been shown in the paper by Treysséde et al. [23] that a simple weak formulation of Equation (5) produces spurious modes when Lagrangian elements are used. To avoid this, a mixed finite element formulation was proposed. This mixed formulation is based on the two variables, pressure and displacement, which satisfy the inf-sup condition in the no-flow case. Then, the mixed formulation, which is an analogous formulation to Equation (5), can be written as

$$\begin{aligned} -\rho_0\omega^2\boldsymbol{w} - 2i\omega\rho_0\boldsymbol{v}_0 \cdot \boldsymbol{\nabla}\boldsymbol{w} + \rho_0\boldsymbol{v}_0 \cdot \boldsymbol{\nabla}(\boldsymbol{v}_0 \cdot \boldsymbol{\nabla}\boldsymbol{w}) + \boldsymbol{\nabla}p &= \boldsymbol{0} \\ p + \rho_0 c_0^2 \boldsymbol{\nabla} \cdot \boldsymbol{w} &= 0. \end{aligned} \tag{8}$$

To obtain a variational form of Equation (8), we introduce test functions $\boldsymbol{w}^*$ and p^*. The result of the weak formulation as given in [23] assumes a divergence-free flow field $\boldsymbol{v}_0$, i.e., $\nabla \cdot \boldsymbol{v}_0 = 0$. This assumption, which is part of the necessary hypotheses for an incompressible fluid, should be valid even for air provided separation of scales holds. With the domain Ω and the boundary Γ, integration

by parts leads to the weak formulation of the Galbrun equation:

$$
\begin{aligned}
&-\int_\Omega \frac{1}{\rho_0 {c_0}^2} p^* p \, d\Omega + \int_\Omega \boldsymbol{\nabla} p^* \cdot \boldsymbol{w} \, d\Omega + \int_\Omega \boldsymbol{w}^* \cdot \boldsymbol{\nabla} p \, d\Omega - \omega^2 \int_\Omega \rho_0 \boldsymbol{w}^* \cdot \boldsymbol{w} \, d\Omega \\
&-i\omega \int_\Omega \rho_0 \boldsymbol{w}^* \cdot (\boldsymbol{v}_0 \cdot \boldsymbol{\nabla} \boldsymbol{w}) \, d\Omega + i\omega \int_\Omega \rho_0 (\boldsymbol{v}_0 \cdot \boldsymbol{\nabla} \boldsymbol{w}^*) \cdot \boldsymbol{w} \, d\Omega \\
&- \int_\Omega \rho_0 (\boldsymbol{v}_0 \cdot \boldsymbol{\nabla} \boldsymbol{w}^*) \cdot (\boldsymbol{v}_0 \cdot \boldsymbol{\nabla} \boldsymbol{w}) \, d\Omega + \int_\Gamma \boldsymbol{w}^* \cdot \left[\rho_0 (\boldsymbol{v}_0 \cdot \boldsymbol{n}) \frac{d\boldsymbol{w}}{dt} \right] d\Gamma \\
&- \int_\Gamma p^* (\boldsymbol{w} \cdot \boldsymbol{n}) \, d\Gamma = 0, \qquad\qquad \forall \{\boldsymbol{w}^*, p^*\}.
\end{aligned} \tag{9}
$$

The first four terms represent the no-flow case, the following three are added in the ambient flow case, and the last two are the boundary integrals appearing due to integration by parts. The terms with ω^2 and ω will later lead to the mass and damping matrices, respectively, and the remaining integrals contribute to the stiffness matrix. Up to this point, the left-hand side of Equation (9) results in a quadratic polynomial matrix.

In computations with flow limited to domains with rigid walls and absorbing walls with zero flow in normal direction, the normal components of the ambient flow $\boldsymbol{v_0} \cdot \boldsymbol{n}$ are equal to zero on the boundary. Hence, the first boundary integral vanishes in such a case. The second boundary integral of Equation (9) vanishes for rigid boundary conditions (cf. Equation (6)). Frequency dependence of the boundary admittance controls whether the contribution of the second boundary integral is added to mass, stiffness or damping matrix, or even if it results in a new term. For instance, a frequency independent boundary admittance results in a matrix proportional to $1/\omega$. Thus, in this case, the polynomial matrix becomes cubic (cf. Equation (11), below).

In case of rigid walls, Equation (9) results in a quadratic eigenvalue problem as

$$
-\omega^2 \boldsymbol{M}\boldsymbol{u} - i\omega \boldsymbol{D}\boldsymbol{u} + \boldsymbol{K}\boldsymbol{u} = \boldsymbol{0}, \tag{10}
$$

with $\boldsymbol{u}$ comprising displacement and pressure degrees of freedom. The mass matrix $\boldsymbol{M}$ and the stiffness matrix $\boldsymbol{K}$ are symmetric and real, the damping matrix $\boldsymbol{D}$ is skew-symmetric. In this mixed formulation, mass and damping matrices, both are singular because neither of them include entries connected to the pressure terms.

In case of frequency independent admittance boundary conditions, Equation (9) results in a cubic eigenvalue problem as

$$
-\omega^3 \boldsymbol{M}\boldsymbol{u} - i\omega^2 \boldsymbol{D}\boldsymbol{u} + \omega \boldsymbol{K}\boldsymbol{u} + \boldsymbol{A}\boldsymbol{u} = \boldsymbol{0}. \tag{11}
$$

Matrices $\boldsymbol{M}$, $\boldsymbol{D}$ and $\boldsymbol{K}$ are the same as above. Usually, $\boldsymbol{A}$ is sparse and complex.

The eigenvalue problem is set up and solved by using the commercial codes COMSOL Multiphysics [4] and MATLAB [15]. While the quadratic eigenvalue problem is solved within MATLAB using command `eigs`, the cubic eigenvalue problem is solved iteratively within COMSOL.

2.3. Types of finite elements

Herein, different types of finite elements are investigated. Their choice is mainly motivated by the selection of finite elements in the papers by Treysséde et al. [23] and Gabard et al. [7]. Behavior of standard Lagrangian elements is demonstrated for comparison only. The discussion of elements is limited to the two-dimensional case. However, all of these element types are known for three dimensional applications as well. In what follows, elements will be referred to by their names and by abbreviations as used in [7] and shown in Figure 1.

2.3.1. Lagrangian elements Standard Lagrangian elements are well-known. They represent the most commonly used type of finite elements; see for example [2, 24]. Herein, only linear triangular elements as shown in Figure 1(a) are used. All nodes of the element are equipped with displacement and with pressure degrees of freedom. This element type will also be referred to as T3–3c.

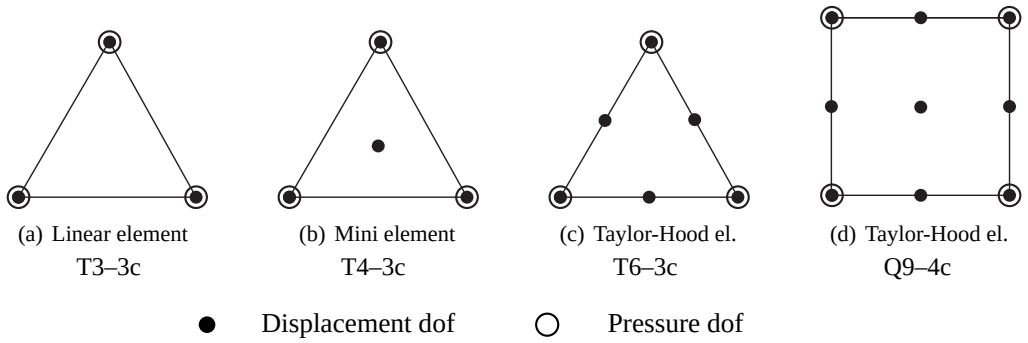

Figure 1. Element types which have been used to solve the eigenvalue problem.

2.3.2. Mini elements Similar to Lagrangian elements, Mini elements are triangular elements with displacement and pressure degrees of freedom at their three vertices (cf. Figure 1(b)). In addition to these nine degrees of freedom, another two degrees of freedom for the displacement are linked with a fourth node in the barycenter of the element. The associated basis functions are known as bubble functions since they vanish along all edges of the element. The abbreviation for this element is T4–3c.

2.3.3. Taylor-Hood elements A combination of linear approximation for pressure and quadratic approximation for displacement is known as Taylor-Hood element. Treysséde et al. [23] and Gabard et al. [7] tested quadrilateral elements as shown in Figure 1(d). To achieve a better comparison with the triangular Mini elements, triangular Taylor-Hood elements are tested as well (cf. Figure 1(c)). As shown, the Taylor-Hood elements will be referred to as T6–3c and Q9–4c.

2.3.4. Other elements For this study, the authors have tested a number of additional higher order elements similar to Taylor-Hood-like elements, e.g. T10–6c and Q25–16c. Since they behave similar to Taylor-Hood elements shown in Figures 1(c) and 1(d), a detailed description of these test cases is omitted.

3. COMPUTATIONAL EXAMPLE I: THE LONG DUCT

3.1. Model description

We consider a similar example as in [13] (for the no-flow case). It consists of a fluid-filled duct of length L and width H such that $H << L$. We assume that the duct domain covers the area of $0 \leq x \leq L$ and $0 \leq y \leq H$ (cf. Figure 2). The ambient flow velocity $\boldsymbol{v}_0$ reduces to a (positive) component v_{0x}, whereas the orthogonal component vanishes: $v_{0y} = 0$. Then, the Mach number is $Ma = v_{0x}/c_0$. Since we compare solutions of the two-dimensional method with the analytical solution of the corresponding one-dimensional problem, it is necessary to apply zero boundary conditions to all surfaces as in Equation (6).

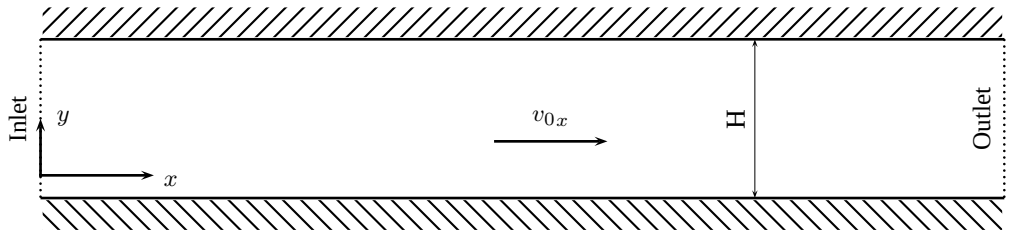

Figure 2. Geometry of the duct.

3.2. Analytical solution

It is possible to derive an analytical solution of the Galbrun equation for a one-dimensional duct with constant ambient velocity. An infinite duct has a continuous spectrum of eigenvalues. In order to have a discrete spectrum, we solve the problem on the interval $(0, L)$ with the boundary conditions $w_x(0) = 0$ and $w_x(L) = 0$. In this case, these boundary conditions do not represent rigid walls, which would physically contradict the condition of a constant velocity, but they represent nodes imposed to the eigenvectors. Notice that, in such a case, the boundary term $\int_\Gamma \boldsymbol{w}^* \cdot \left[\rho_0(\boldsymbol{v}_0 \cdot \boldsymbol{n})\frac{d\boldsymbol{w}}{dt}\right] d\Gamma$ from Equation (9) does not appear either, because the test functions $\boldsymbol{w}^*$ vanish on the inlet and the outlet of the duct. Thus, a discrete spectrum of eigenvectors with wavelengths $\lambda = 2L,\, 3/2L,\, L,\, L/2, \ldots$ is extracted from the original continuous spectrum. The eigenvalues for the circular frequency ω_n and the frequency f_n are real and yield

$$\omega_n = \frac{c_0 \pi n}{L}\left(1 - Ma^2\right), \quad \text{i.e.,} \quad f_n = \frac{c_0 n}{2L}\left(1 - Ma^2\right). \tag{12}$$

The solution corresponds to that of the no-flow case diminished by the term Ma^2. The first three eigenfrequencies as functions of the Mach number are depicted in Figure 3.

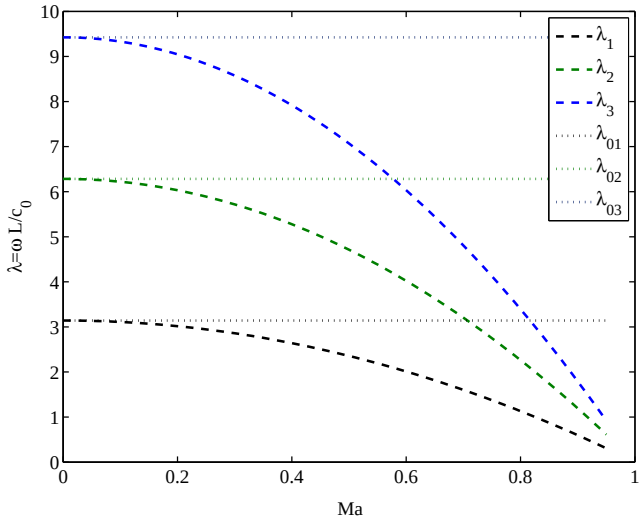

Figure 3. Duct: First three eigenfrequencies in terms of Ma.

Contrary to the eigenvalues, the eigenvectors are complex:

$$w_n = C\left[e^{-i\frac{\pi n}{c_0 L}(v+c_0)x} - e^{-i\frac{\pi n}{c_0 L}(v-c_0)x}\right]. \tag{13}$$

Here and below, C is chosen in such a way that the first real maximum amplitude on the domain equals 1. The behavior of the real and the imaginary parts are depicted in Figure 4. Their amplitudes increase and decrease periodically. Notice that real and imaginary parts exhibit the same behavior shifted in phase.

3.3. Numerical results

In this subsection, it will be clarified whether the elements, depicted in Figure 1, are suitable to solve the eigenvalue problem or if it is necessary to look for alternative elements. It turns out that the applicability of elements strongly depends on the Mach number. This behavior has already been noticed in former studies [6, 8, 18, 22, 23], but none of these explicitly addresses the eigenvalue problem; the main focus within their studies was on the propagation of acoustic waves. Herein, a classification of the elements will show at which Mach numbers each of them can be reasonably

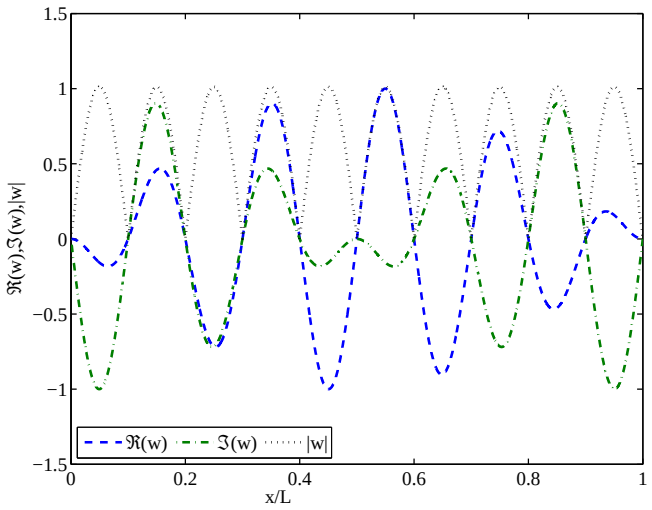

Figure 4. Duct: Behavior of $\Re(w_x)$ and $\Im(w_x)$ along the duct.

employed. The notion of stability of an element has to be redefined. In what follows, an element is denoted to be *stable* if the exact solutions (cf. Equation (12)) can be clearly identified in the numerical spectrum. Otherwise, if the field of regular solutions is polluted by parasitic values, the element is defined to be *unstable*.

The domain used for this study has a length of 3.4 m and its width is set to 0.05 m. This high ratio of side lengths is chosen to maximize the number of regular modes which are only related to the length of the duct. The speed of sound and mass density are assumed to be $c_0 = 340\,\mathrm{m/s}$ and $\rho_0 = 1.2\,\mathrm{kg/m^3}$ respectively. Hence, the expected eigenfrequencies corresponding to the one-dimensional duct in the no-flow case are $f = 0\,\mathrm{Hz}$, 50 Hz, 100 Hz, 150 Hz, and so on (cf. [13]). The corresponding circular frequencies are $\omega_k = 100\pi k\,\mathrm{Hz}$, with $k = 0, 1, 2, \ldots$

To analyze the appearance of spurious eigenvalues more closely, multiple test scenarios have been developed. For this, the Mach number is increased in three steps. We consider the cases of $Ma = 0$, $Ma = 0.1$, $Ma = 0.5$ and $Ma = 0.9$. Within each step, the computation of the eigenvalue problem is carried out on two different meshes for each element type depicted in Figure 1. Table I provides a brief survey of the different meshes that we have used and the corresponding problem sizes, i.e., the number of degree of freedom (dof). These four meshes are depicted in Figure 5.

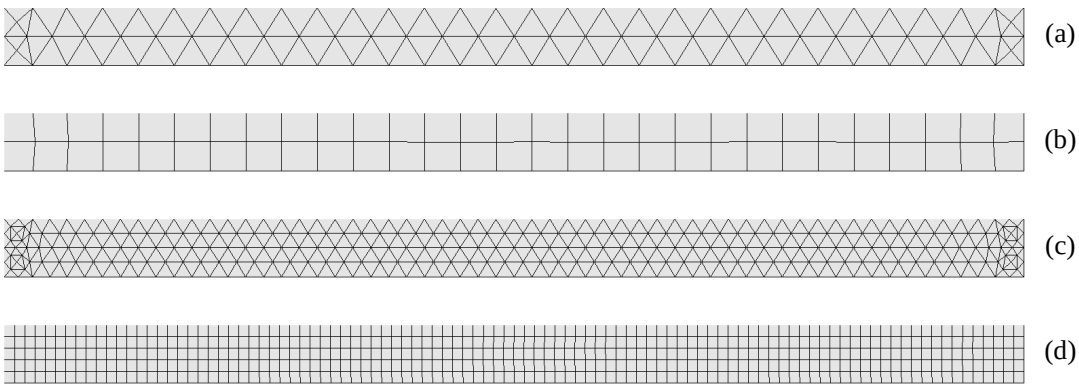

Figure 5. Duct meshed by triangular (a,c) and quadrilateral elements (b,d), coarse grid representing mesh case 1 (a,b), finer grids representing mesh case 2 (c,d).

Table I. Duct: Test cases which will be applied to each element depicted in Figure 1. The number of elements is declared by n_{el} and "dof" represents the number of degrees of freedom.

	Mesh case 1		Mesh case 2	
	n_{el}	dof	n_{el}	dof
T3–3c	126	285	504	945
T4–3c	126	537	504	1953
T6–3c	126	725	504	2581
Q9–4c	58	680	500	5028

The first test case deals with the no-flow case, i.e., the case of $Ma = 0$. This investigation is chosen to confirm that Lagrangian elements are not suited to be applied to Equation (9). With this end, the eigenvalues computed by using linear Lagrangian elements (cf. Figure 6(a)) are compared to the solution which is achieved when using Mini elements (cf. Figure 6(b)). Both solutions appear to be purely real. Hardly any error is visible for the Mini elements for which the eigenvalues are equidistantly distributed along the real axis. However, the eigenvalues which are found by using Lagrangian elements seem to be randomly distributed along the real axis. Actually, the correct eigenvalues are evaluated similar to the Mini elements but, additionally, a number of other modes, the so-called spurious modes, are computed. Such spurious modes pollute the solution of the typical boundary value problem as demonstrated by Treyssède et al. [23]. These spurious modes, which occur for the no-flow problem, do not vanish for a Mach number greater than zero. Therefore, Lagrangian elements are not not further taken into account in this study.

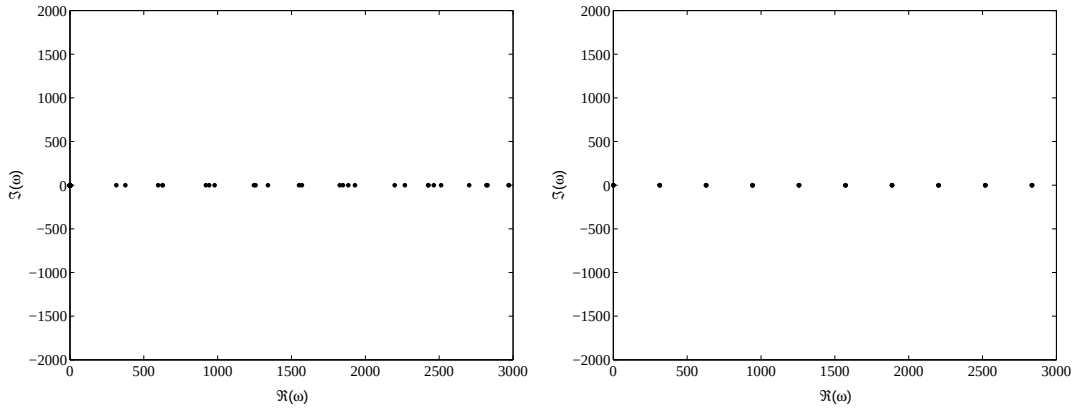

(a) Lagrangian elements (b) Mini elements

Figure 6. Duct: Test case 1: $Ma = 0$, mesh case 2: Comparison of eigenvalues ω_k for Lagrangian elements and Mini elements.

In the second test case, we consider a Mach number $Ma = 0.1$. The eigenvalue distribution of two different meshes of Taylor-Hood triangular elements (T6–3c) is shown in Figure 7. At first glance, both plots show the complex eigenvalues virtually arbitrarily distributed in the complex plane. However, the regularly appearing dots along the real axis correspond to the eigenvalues which have a physical meaning. The eigenvalues of spurious modes are all complex. This behavior is clearly observed for both meshes. A qualitatively similar result is obtained for the other two types of elements, i.e., T4–3c and Q9–4c. In all cases, the spurious modes appear at a certain distance of the physical modes and, apparently, this is the reason why they have not been observed in other studies when solving the boundary value problems in [7, 8, 22, 23].

Eigenvalues of the quadratic eigenvalue problem (cf. Equation (10)) occur either as real values or as conjugate complex pairs. Consequently, the distribution of eigenvalues in the complex plane should be symmetric with respect to the real axis. Results in Figure 7, and later on in Figures 9,

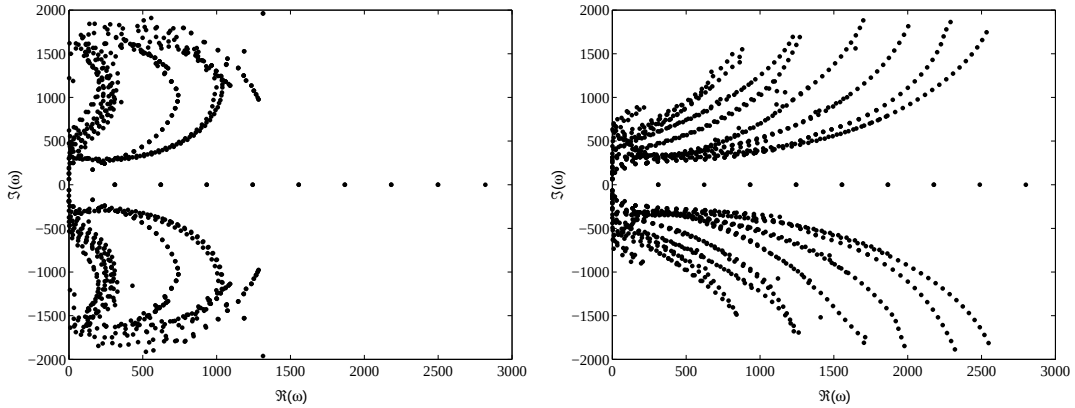

(a) Mesh case 1: 725 dof (b) Mesh case 2: 2581 dof

Figure 7. Duct: Test case 2: $Ma = 0.1$, Taylor-Hood elements T6–3c, eigenvalue distribution for two meshes (cf. Table I).

10, and 11, show essentially symmetric distributions. However, at a close up they are not entirely symmetric, which is likely due to numerical approximation errors. At least, numerous computations confirm the location and uniqueness of eigenvalues along and close to the real axis and a generally correct distribution of the remaining ones.

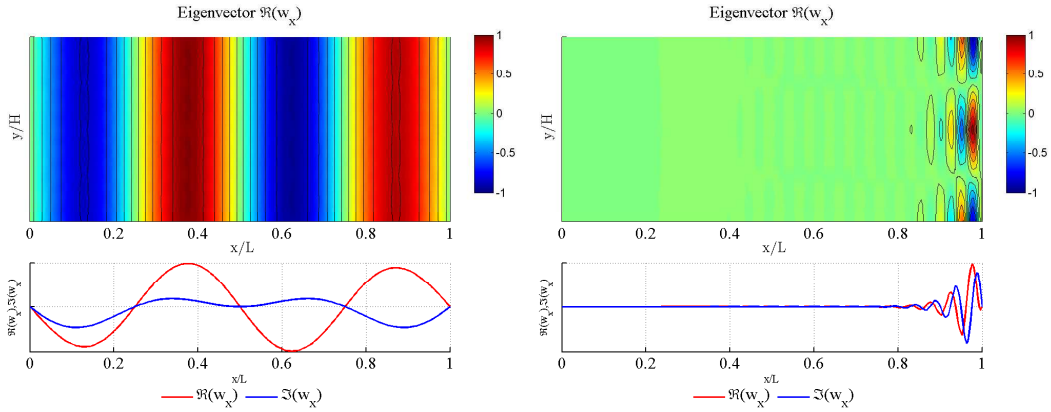

(a) $f = 198\,\mathrm{Hz}$ (b) $f = (193.4 + 74.7i)\,\mathrm{Hz}$

Figure 8. Duct: Test case 2: $Ma = 0.1$, Taylor-Hood elements T6–3c: Eigenvectors for w_x of a physical (left) and a spurious (right) mode close to 195 Hz. The lower parts show cross-plots along the line of symmetry of the upper parts, i.e., along $y = H/2$.

It is not really practical, but at least possible, to identify physical and spurious modes based on a visual impression of the eigenvectors. Figure 8 allows us to compare two eigenmodes with adjacent frequencies around $f = 195\,\mathrm{Hz}$. In this case, the T6–3c elements are used on the finer mesh (i.e., mesh case 2). In the lower part of Figure 8(a), the real and imaginary parts of the fourth mode of the numerical solution match well with the exact solutions (cf. Equation (13)). All outputs are scaled such that the greatest magnitude equals one. The spurious mode in Figure 8(b) is not only identified by its complex eigenfrequency of $f = 193.4 + 74.7i\,\mathrm{Hz}$, as shown. It clearly contains high frequency waves which are not physical for a frequency of approximately 195 Hz. A rough estimate is always possible by using the equation $\lambda = c/f$. Of course, this estimate holds for the no-flow case. But it is easily applicable for low Mach numbers as well.

Greater Mach numbers are studied in a third test case. Figures 9, 10, and 11 show the eigenvalue distributions for the Mini elements (T4–3c), triangular (T6–3c), and quadrilateral (Q9–4c) Taylor-Hood elements. These results are found for the mesh case 2, i.e., for the finer mesh.

The eigenvalue distribution of the solution using Mini elements confirms the observations of Gabard et al. [7]. Therein, the authors stated that the Mini elements perform stable up to a Mach number of 0.5. Beyond this, the solution may become unstable. This is clearly confirmed in Figure 9(b). While the eigenvalues on the real axis are still evenly distributed in Figure 9(a) numerous additional and unwanted eigenvalues are observed in Figure 9(b). There is no doubt that Mini elements are not suited for solution of the boundary value problem for Mach numbers approaching 1. We are not clarifying the limit though.

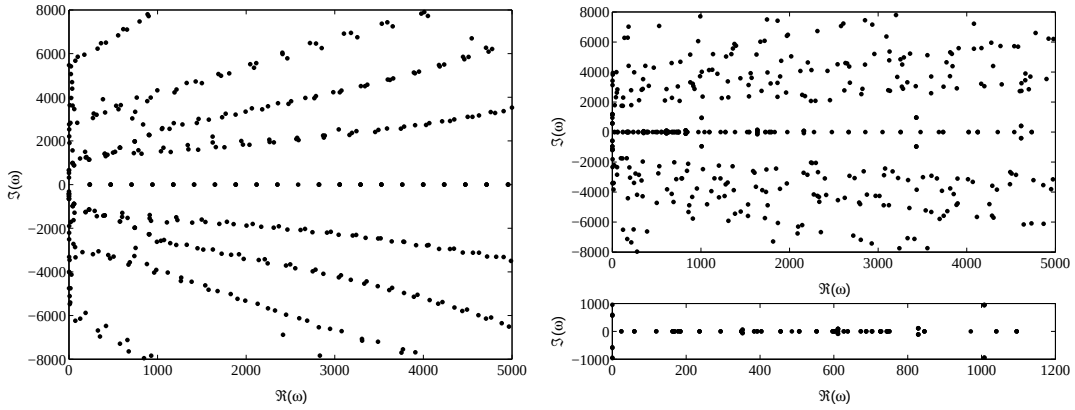

(a) $Ma = 0.5$ (b) $Ma = 0.9$

Figure 9. Duct: Test case 3: Mini elements T4–3c, mesh case 2, eigenvalue distribution for two Mach numbers.

The situation is different for both variants of Taylor-Hood elements. Both, triangular (cf. Figure 10) and quadrilateral (cf. Figure 11) elements, clearly distinguish eigenvalues on the real axis from the other ones. Again, eigenvalues on the real axis account for the physically relevant ones whereas complex eigenvalues are associated to spurious modes. For Mach numbers of 0.9, the spacing between the eigenvalues decreases dramatically. While the fourth non-zero eigenfrequency of the no-flow case is found at 200 Hz, and thus its circular frequency ω lies beyond 1200 Hz, for a Mach number of 0.9 we expect 20 of them with circular frequencies below 1200 Hz (cf. Equation 12). In the lower part of Figure 10(b), we count 18 dots up to a circular frequency of 1200 Hz, whereas, in that of Figure 11(b), the actual number of 20 dots is identified. The increasing number of modes within a particular frequency range leads to significantly decreasing frequencies for which the mesh can be used.

Many applications require determination of the lowest eigenvalues. Therefore, it is important to know up to which frequency the finite elements give accurate results. For that, we define the relative error as

$$e^{\mathrm{rel}} = \left| \frac{\omega^{\mathrm{num}} - \omega^{\mathrm{ex}}}{\omega^{\mathrm{ex}}} \right| \tag{14}$$

where ω^{num} represents the numerical solution and ω^{ex} the analytical solution of the one-dimensional problem.

Assuming the rule of thumb $kh < 1$ (cf. [11, 12]), we would expect our finer meshes (i.e., mesh case 2) to allow more than 9.5 waves along the duct ($f < 950\,\mathrm{Hz}$ in the no-flow case) for the triangles and almost 16 ($f < 1590\,\mathrm{Hz}$ in the no-flow case) for the quadrilaterals. Tables II, III, and IV survey the maximum eigenfrequencies for which the numerical solution remains below a certain error for the finite elements that we are considering. Since the wavelength shortens for increasing Mach number, the right-hand parts of these tables contain the maximum number of waves in the duct to remain below this certain error in the eigenfrequency.

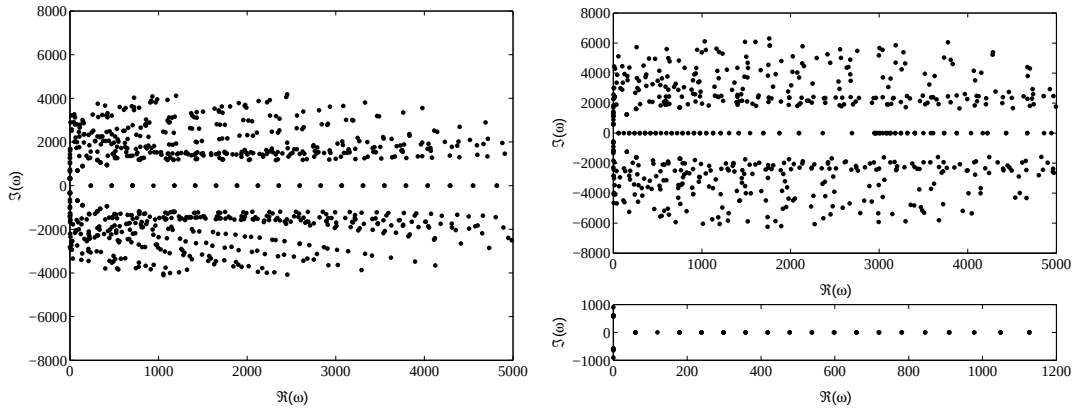

(a) $Ma = 0.5$ (b) $Ma = 0.9$

Figure 10. Duct: Test case 3: Taylor-Hood elements T6–3c, mesh case 2, eigenvalue distribution for two Mach numbers.

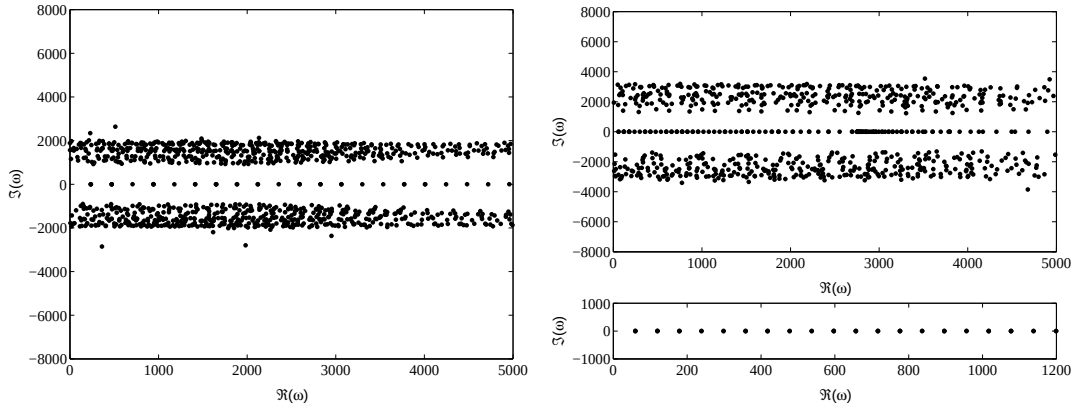

(a) $Ma = 0.5$ (b) $Ma = 0.9$

Figure 11. Duct: Test case 3: Taylor-Hood elements Q9–4c, mesh case 2, eigenvalue distribution for two Mach numbers.

Table II. Duct: Mesh case 2, Mini elements T4–3c: Limitations of element type.

	Maximum eigenfrequency f in Hz for			Maximum number of waves for		
Ma	$e^{\text{rel}} \leq 0.01\%$	$e^{\text{rel}} \leq 0.1\%$	$e^{\text{rel}} \leq 1\%$	$e^{\text{rel}} \leq 0.01\%$	$e^{\text{rel}} \leq 0.1\%$	$e^{\text{rel}} \leq 1\%$
0	50	250	850	0.5	2.5	8.5
0.1	198	396	891	2	4	9
0.5	75	262	562	1	3.5	7.5
0.9	0	10	19	0	0.5	1

Table III. Duct: Mesh case 2, Taylor-Hood elements T6-3c: Limitations of element type.

	Maximum eigenfrequency f in Hz for			Maximum number of waves for		
Ma	$e^{\text{rel}} \leq 0.01\%$	$e^{\text{rel}} \leq 0.1\%$	$e^{\text{rel}} \leq 1\%$	$e^{\text{rel}} \leq 0.01\%$	$e^{\text{rel}} \leq 0.1\%$	$e^{\text{rel}} \leq 1\%$
0	250	550	950	2.5	5.5	9.5
0.1	346	594	940	3.5	6	9.5
0.5	262	412	638	3.5	5.5	8.5
0.9	48	86	124	2.5	4.5	6.5

Table IV. Duct: Mesh case 2, Taylor-Hood elements Q9–4c: Limitations of element type.

	Maximum eigenfrequency f in Hz for			Maximum number of waves for		
Ma	$e^{\mathrm{rel}} \leq 0.01\%$	$e^{\mathrm{rel}} \leq 0.1\%$	$e^{\mathrm{rel}} \leq 1\%$	$e^{\mathrm{rel}} \leq 0.01\%$	$e^{\mathrm{rel}} \leq 0.1\%$	$e^{\mathrm{rel}} \leq 1\%$
0	450	850	950	4.5	8.5	9.5
0.1	594	891	940	6	9	9.5
0.5	412	675	825	5.5	9	11
0.9	76	133	218	4	7	11.5

3.4. Duct with admittance boundary conditions at end caps

Eigenvalues of the system with admittance boundary conditions at end caps can be analytically found when the condition of Equation (7) is used. Obviously, this condition is not valid for a physically realistic model since it neglects the fact that the end caps are inlet and outlet of the duct. The solution would be very similar to the one in [13]. This means, that for the formulation used in this paper, the complex eigenvalues have a small but constant imaginary part. Hardly any difference in comparison to the non-dissipative system will be observed. For this reason, the example of the duct with admittance boundary conditions at end caps will not be discussed in detail in this work.

4. COMPUTATIONAL EXAMPLE II - ANNULUS WITH ABSORBING BOUNDARY

4.1. Model description

We consider an annulus domain for our the second computational example. Again, we use the material data of air, i.e., $c_0 = 340\,\mathrm{m/s}$ and $\rho_0 = 1.2\,\mathrm{kg/m^3}$. The domain is bounded by an inner and an outer circle of radius r_1 and r_2, respectively (cf. Figure 12). The radii of the inner and the outer circle are set to be 0.75 and 1.0 m, respectively.

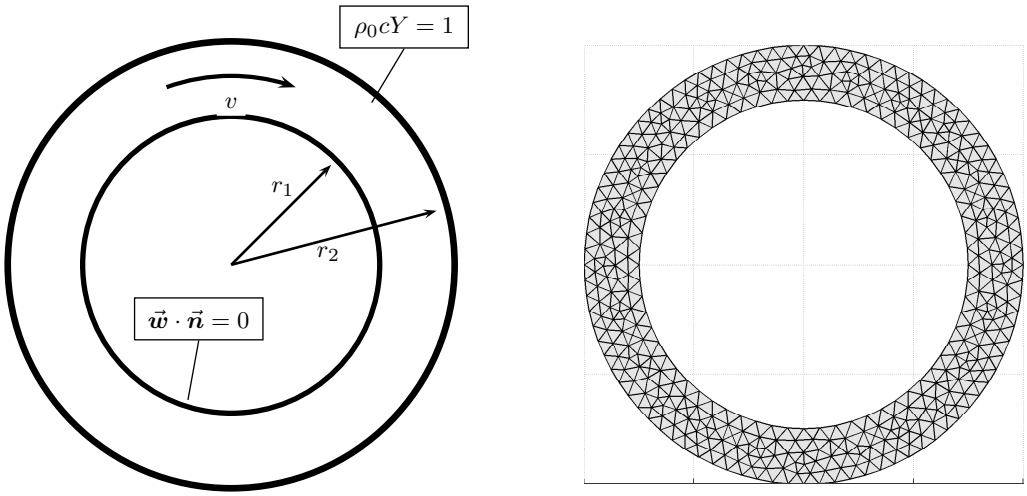

Figure 12. Annulus: Domain and mesh of the two-dimensional problem.

We further assume a steady ambient flow in circumferential direction. The velocity profile is assumed to be linear in terms of the radius as

$$\boldsymbol{v} = \begin{bmatrix} v_r \\ v_\varphi \end{bmatrix} = \begin{bmatrix} 0 \\ r\omega_\varphi \end{bmatrix}, \tag{15}$$

with ω_φ being the (constant) angular velocity of the flow. We will refer to the Mach number as the flow velocity at the outer boundary related to the speed of sound. Hence, $Ma = v_\varphi(r_2)/c_0$. For the

inner boundary, we assume the boundary condition is as in Equation (6):

$$w_r(r_1) = 0. \tag{16}$$

Again, this boundary condition represents a rigid (i.e., fully reflecting) wall. The condition at the outer boundary represents absorption, but does not aim at a non-reflecting boundary condition. However, the boundary condition is chosen such that the distribution of eigenvalues of physical and spurious modes is comparable to the situation for a discretized exterior problem similar to [5]. With respect to Equation (7), we use

$$\rho_0 c_0 Y = \tilde{Y} = 1 \tag{17}$$

and, thus,

$$-i\omega\rho_0 c_0 \boldsymbol{w}_r(r_2) = p(r_2). \tag{18}$$

Different from the tests in the previous section, only triangular Taylor-Hood elements (T6–3c) are used for the analysis of the annulus. This restriction is used since Mini elements have shown limitations in the previous example. Quadrilateral Taylor–Hood elements (Q9–4c) are not reported because they behave similarly to the triangular ones.

The finite element model of the annulus consists of 786 triangular T6–3c elements (cf. Figure 12 (right)). This results in 469 nodes and 3917 degrees of freedom. Note that a cubic eigenvalue problem results in three eigenvalues per degree of freedom. However, fewer eigenvalues are determined since the leading matrix and the frequency independent matrix $\boldsymbol{A}$ are both singular. The cubic eigenvalue problem is solved iteratively within the software COMSOL Multiphysics [4].

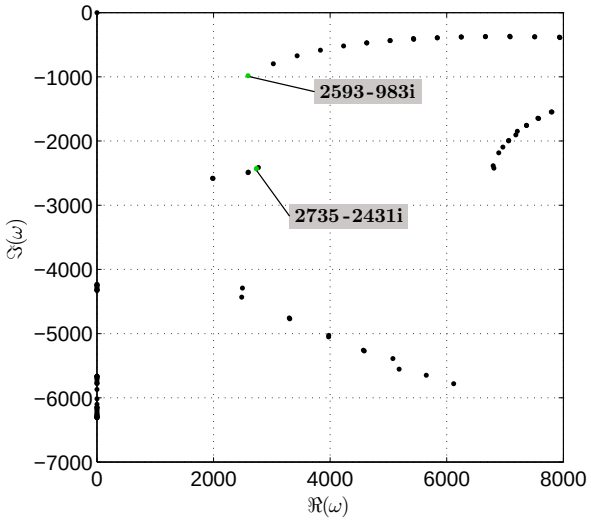

Figure 13. Eigenvalue distribution for $Ma = 0$.

In order to obtain a reference eigenvalue distribution, the eigenvalue problem is solved for the no-flow case first, i.e., $Ma = 0$. Figure 13 shows the eigenvalues of lowest magnitude. Clearly, the spectrum is free of spurious modes as expected for the no-flow case (i.e., a mixed finite element solution of the Helmholtz equation). Some of the modes, in particular purely imaginary modes and modes in the region determined by $1900 < \Re(\omega) < 2800$ and $2400 < \Im(\omega) < 2600$ look like the basic modes of external problems, as identified in [14]. These are the monopole (eigenvalue $2769 - 2412i$), two dipoles ($2735 - 2431i$), two quadrupoles ($2595 - 2488i$) and two hexapoles ($1988 - 2581i$). Other modes look more like standing waves in circumferential direction. Low order modes are missing, the first of these modes (eigenvalue $2593 - 983i$) shows five waves over the circumference. Subsequent modes with eigenvalues $3025 - 797i$ and $3434 - 673i$ consist of six and

seven waves, respectively. In comparison to [14], it is worth mentioning that, real eigenvalues in our paper can be compared with imaginary eigenvalues in the former one. Recall that eigenvectors can be scaled arbitrarily. One dipole mode and the circumferential mode of five waves are depicted in Figure 14. These modes correspond to the green dots indicating their eigenvalues in the complex plane in Figure 13. Note that only the sound pressure component is shown in Figure 14.

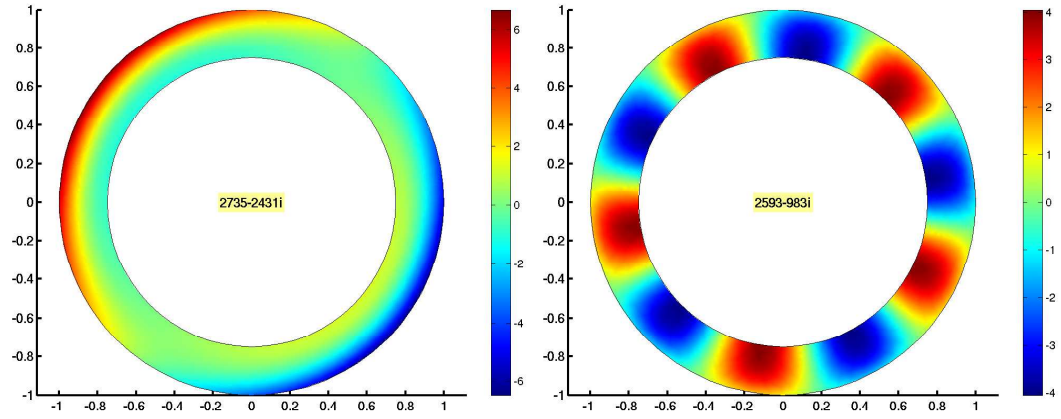

Figure 14. Two arbitrarily chosen eigenvectors (sound pressure component only) for the case $Ma = 0$, dipole mode (left) and mode with five circumferential waves (right); eigenvalue shown in the center of the annulus.

Similar to the duct case, the Mach number is increased in three steps. Again, we consider the cases of $Ma = 0.1, Ma = 0.5$ and $Ma = 0.9$.

For $Ma = 0.1$ (cf. Figure 15), the distribution of physical eigenvalues in the complex plane is polluted by spurious modes. However, it is still possible to make assumption on which modes might be physical. In particular, the right-hand part of the graph seems to be free of spurious solutions. Low order modes, however, must be sought among numerous false eigenvalues. As an example, Figure 15, shows the eigenvalues of two physical (green) and two spurious modes (red) which are located closely together. The mode shapes are depicted in Figure 16 for the physical and in Figure 17 for the spurious modes. A distinction between them is possible with respect to the acoustic wavelength. The modes in Figure 16 are identified by the wavelength λ which is close to $\lambda = c/f_i$ with frequency $f_i = \Re\{\omega_i/(2\pi)\}$ (where ω_i represents the eigenvalue) and the effective speed of sound given by $c = c_0 \pm v_0$. Spurious modes are identified by shorter wavelengths as shown in Figure 17. However, it is not clear whether this criterion can be used as a general one.

For $Ma = 0.5$ and $Ma = 0.9$ (cf. Figure 18), spurious solutions are spread all over the shown interval. A visual distinction between physical and spurious modes is almost impossible. In both subfigures, two physical and two spurious solutions are marked in green and red, respectively. The corresponding physical modes are depicted in Figure 19 for $Ma = 0.5$ and in Figure 20 for $Ma = 0.9$. Identification of physical modes based on their wavelengths is still possible. For instance, Figure 20 (right) corresponds to a distorted dipole mode. The distortion results from the flow field. In addition to the physical modes, an investigation of the spurious ones which are marked in Figure 18 has shown a similar pressure distribution as in Figure 17. Finally, the authors find it worth mentioning that for $Ma = 0.9$ (cf. Figure 18 (right)), the eigenvalues closest to the real axis with $1200 < \Re(\omega) < 3000$ are all physical modes.

5. CONCLUSIONS

In this study, the acoustic eigenvalue problem in the presence of an ambient flow described by Galbrun equation is analyzed numerically using a mixed finite element formulation. The results of eigenvalues and eigenvectors for a straight duct and for an annulus with an absorbing wall are discussed.

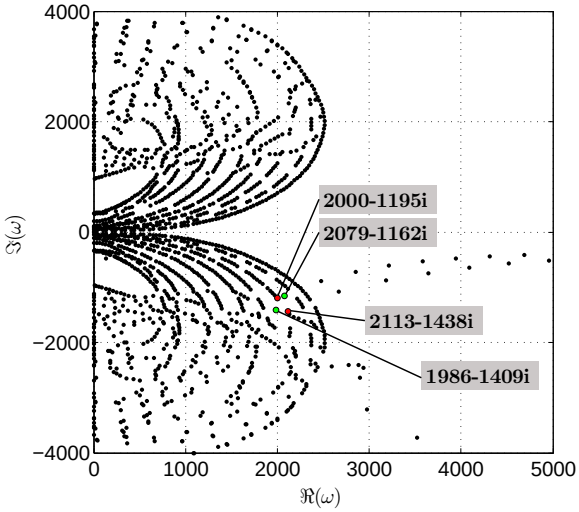

Figure 15. Eigenvalue distribution for $Ma = 0.1$.

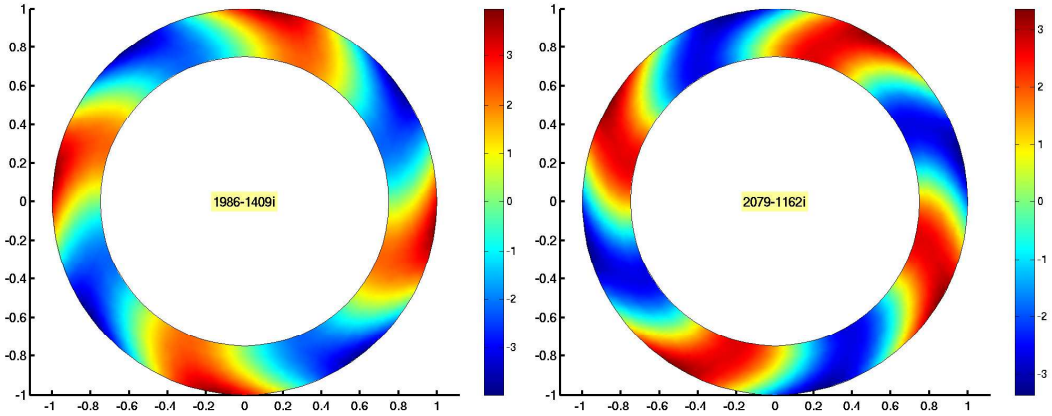

Figure 16. Sound pressure component of two physical modes for $Ma = 0.1$; eigenvalue shown in the center of the annulus.

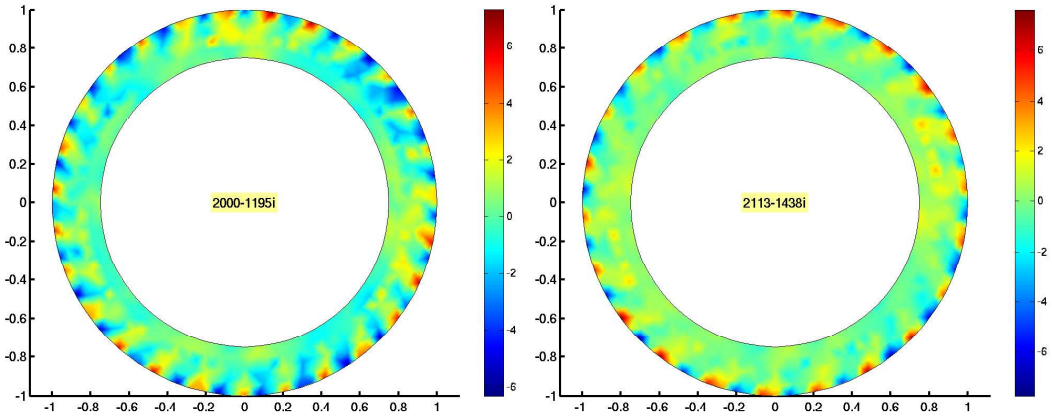

Figure 17. Sound pressure component of two spurious modes for $Ma = 0.1$; eigenvalue shown in the center of the annulus.

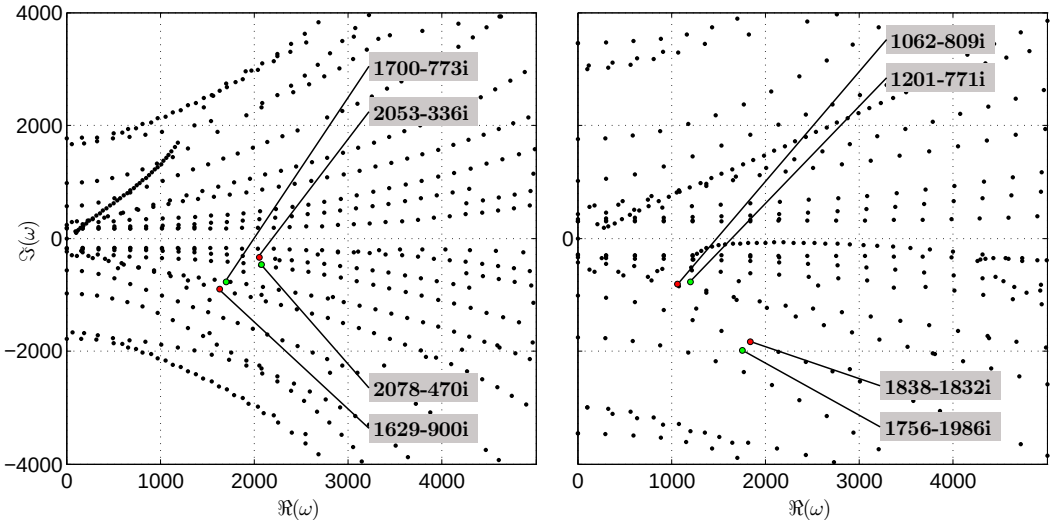

Figure 18. Eigenvalue distribution for $Ma = 0.5$ (left) and $Ma = 0.9$ (right).

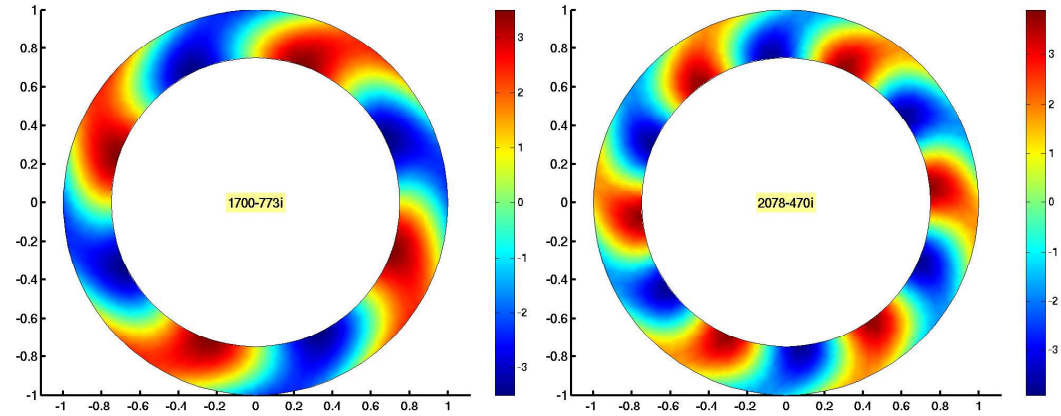

Figure 19. Sound pressure component of two physical modes for $Ma = 0.5$; eigenvalue shown in the center of the annulus.

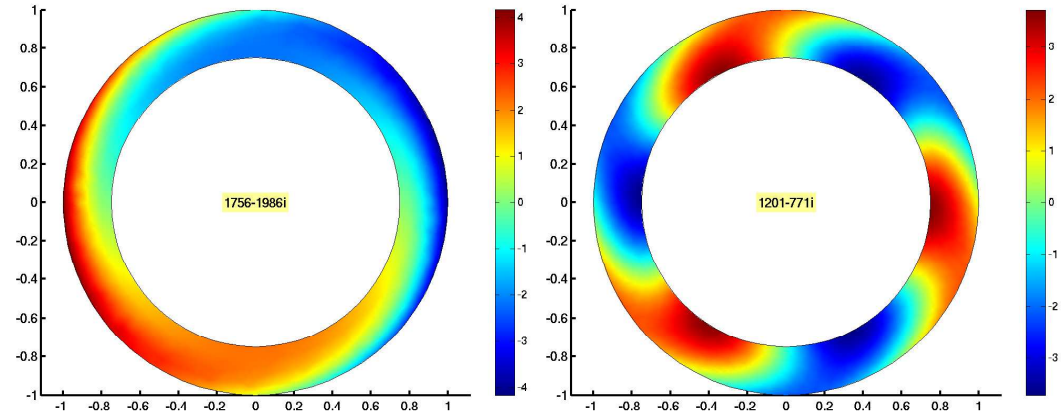

Figure 20. Sound pressure component of two physical modes for $Ma = 0.9$; eigenvalue shown in the center of the annulus.

In the case of the energy conserving duct problem, our study basically confirms former results available in the literature. For Mach numbers up to 0.5, Mini elements seem to perform reliably, whereas, for higher flow velocities, even real spurious eigenvalues occur. Taylor-Hood elements, both triangular and quadrilateral, seem to perform robustly even for a Mach number 0.9. However, except for the no-flow case, there are always spurious modes in the system. A problem with purely real eigenvalues or eigenvalues with a small imaginary part can be safely analyzed in frequency domain since the physical and spurious modes are well separated from each other. This explains why Taylor-Hood elements have produced reliable solutions in literature.

The situation is different for exterior problems. The configuration of the annulus is similar to that of an exterior problem, which is confirmed by the shape of the modes in the no-flow case. Again, Taylor-Hood elements produce spurious modes except for the no-flow case. Different from the duct example, physical and spurious modes can hardly be separated now. For a simple case as herein discussed, it seems possible to identify physical modes manually. Such a spatial filter technique could even be automated. However, it cannot account for a reasonable solution of exterior problems of Galbrun equation, because evaluation of a large number of eigenvalues for real applications is not realistic.

The main conclusion is the need of developing a suitable finite element satisfying the inf-sup condition and, hence, spurious modes free.

ACKNOWLEDGMENTS

Three authors (F.D., R.R, and H.W.) were supported by FONDAP and BASAL projects at the CMM, Universidad de Chile, Chile. Furthermore, traveling activities of three authors (F.D., L.H.-N., and S.M.) were supported by PPP – Acciones Integradas Hispano-Alemanas of the German Academic Exchange Service (DAAD) and the Spanish Ministry of Science.

REFERENCES

1. R. J. Astley. Numerical methods for noise propagation in moving flows with application to turbofan engines. *Acoustical Science and Technology*, 30:227–239, 2009.
2. K.-J. Bathe. *Finite Element Procedures*. Prentice Hall, 1996.
3. H. H. Brouwera and S. W. Rienstra. Aeroacoustics research in europe: The ceas–asc report on 2007 highlights. *Journal of the Acoustical Society of America*, 318:625–654, 2008.
4. COMSOL AB, Stockholm, Sweden. *COMSOL Multiphysics Scripting Guide, version 3.5*, 2008.
5. S. Fuß, S. Hawkins, and S. Marburg. An eigenvalue search algorithm for the modal analysis of a resonator in free space. *Journal of Computational Acoustics*, 19(1):95–109, 2011.
6. G. Gabard, R. J. Astley, and M. Ben Tahar. Stability and accuracy of finite element methods for flow acoustics. i: General theory and application to one-dimensional propagation. *International Journal for Numericals Methods in Engineering*, 63:947–973, 2005.
7. G. Gabard, R. J. Astley, and M. Ben Tahar. Stability and accuracy of finite element methods for flow acoustics. ii: Two-dimensional effects. *International Journal for Numericals Methods in Engineering*, 63:974–987, 2005.
8. G. Gabard, F. Treysséde, and M. Ben Tahar. A numerical method for vibro-acoustic problems with sheared mean flows. *Journal of Sound and Vibration*, 272:991–1011, 2004.
9. H. Galbrun. *Propagation d'une Onde Sonore dans l'Atmosphére et Théorie des Zones de Silence*. Gauthier-Villars, Paris, 1931.
10. O. A. Godin. Reciprocity and energy theorems for waves in a compressible inhomogteneous moving fluid. *Wave Motion*, 25:143–167, 1997.
11. F. Ihlenburg. *Finite Element Analysis of Acoustic Scattering*. Springer, Berlin Heidelberg New York, 1998.
12. S. Marburg. Six boundary elements per wavelength. Is that enough? *Journal of Computational Acoustics*, 10(1):25–51, 2002.
13. S. Marburg. Normal modes in external acoustics. part i: Investigation of the one-dimensional duct problem. *Acta Acustica united with Acustica*, 91:1063–1078, 2005.
14. S. Marburg, F. Dienerowitz, T. Horst, and S. Schneider. Normal modes in external acoustics. part ii: Eigenvalues and eigenvectors in 2d. *Acta Acustica united with Acustica*, 92(1):97–111, 2006.
15. The MathWorks, Inc., Natick, Massachusetts. *MATLAB Reference guide, version 7.6.0*, 2008.
16. B. Nennig, E. Perrey-Debain, and M. B. Tahar. A mode matching method for modelling dissipative silencers lined with poroelastic materials and containing mean flow. *Journal of the Acoustical Society of America*, 128:3308–3320, 2010.

17. B. Nennig, M. B. Tahar, and E. Perrey-Debain. A displacement–pressure finite element formulation for analyzing the sound transmission in ducted shear flows with finite poroelastic lining. *Journal of the Acoustical Society of America*, 130:42–51, 2011.
18. C. Peyret and G. Élias. Finite-element method to study harmonic aeroacoustics problems. *Journal of the Acoustical Society of America*, 110:661–668, 2001.
19. A. D. Pierce. Wave equation for sound in fluids with unsteady inhomogeneous flow. *Journal of the Acoustical Society of America*, 87:2292–2299, 1990.
20. B. Poirée. Les équations de l'acoustique linéaire et non-linéaire dans les fluides en mouvement. *Acustica*, 57:5–25, 1985.
21. A. Richter, J. Stiller, and R. Grundmann. Stabilized discontinuous galerkin methods for flow-sound interaction. *Journal of Computational Acoustics*, 15(1):123–143, 2007.
22. F. Treyssède and M. Ben Tahar. Comparison of a finite element model with a multiple-scales solution for sound propagation in varying ducts with swirling flows. *Journal of the Acoustical Society of America*, 115:2716–2730, 2004.
23. F. Treyssède, G. Gabard, and M. Ben Tahar. A mixed finite element method for acoustic wave propagation in moving fluids based on an eulerian-lagrangian description. *Journal of the Acoustical Society of America*, 113:704 – 716, 2003.
24. O. C. Zienkiewicz and R. L. Taylor. *The Finite Element Method. Volume 1: The Basis*. Butterworth-Heinemann, Oxford, 5 edition, 2000.